UNIVERSITÀ DEGLI STUDI DI PADOVA

Dipartimento di Fisica e Astronomia "Galileo Galilei"

Corso di Laurea in Fisica

Tesi di Laurea

Octupole correlations in ^{110}Xe

Relatori

Dr. José Javier Valiente Dobón

Dr. Rosa María Pérez Vidal

Dr. Andrés Illana Sisón

Laureando

Damiano Stramaccioni

Anno Accademico 2020/2021

Contents

1 Introduction

1.1 Octupole correlations

The existence of nuclei with stable deformed shapes was realized early in the history of nuclear physics. The observation of large quadrupole moments led to the suggestion that some nuclei might have spheroidal shapes, which was confirmed by the observation of rotational band structures and measurements of their properties. For most of the deformed nuclei, a description as an axial- and reflection-symmetric spheroid is adequate to reproduce the excited bands. However, with the first observation of negative-parity states near the ground state, arose the possibility that some nuclei might have a shape asymmetric under reflection, such as a pear shape.

The spheroidal nuclear surface is tipically defined by means of standard deformation parameters $\alpha_{\lambda\mu}$ describing the length of the radius vector pointing from the origin to the surface [1]:

$$R(\theta,\phi) = R_0(1 + \sum_{\lambda=2}^{\lambda_{max}} \sum_{\mu=-\lambda}^{+\lambda} \alpha_{\lambda\mu} Y^*_{\lambda\mu}(\theta,\phi)), \tag{1}$$

where λ denotes the multipole order of the deformation and $Y^*_{\lambda\mu}(\theta,\phi)$ are normalised spherical harmonics. Fig. 1 shows an example of this representation. For axially symmetric shapes with respect to the z axis, all deformation parameters with $\mu \neq 0$ vanish. The remaining deformation parameters $\alpha_{\lambda 0}$ are usually called β_λ.

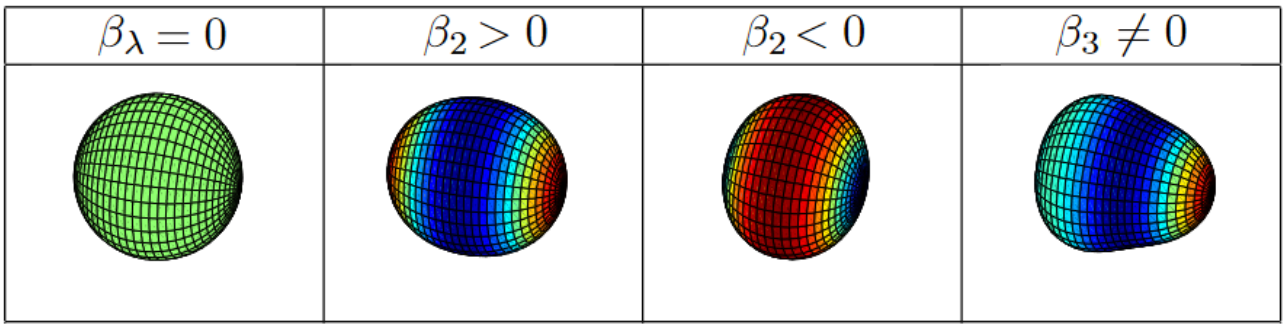

Figure 1: Schematic representation of some typical nuclear shapes, from left to right: spherical, prolate , oblate and reflection-asymmetric octupole shape. Adapted from [2].

From a microscopic perspective the interaction between orbitals of opposite parity differing by three units of total and orbital angular momentum (ΔJ=ΔL=3) gives rise to octupolar deformations, with λ=3. These correlations happen in well-defined areas of the Segré chart, highlighted in Fig. 2, where the number of protons or neutrons is equal to 32, 56, 90, etc. For these cases, nuclei in the region around N = Z are expected to show enhanced octupole correlations, since protons and neutrons occupy identical orbitals. Microscopically, for the mass region around N = Z = 56, the Fermi surface for both protons and neutrons lies between the $d_{5/2}$ and the $h_{11/2}$ orbitals, where the octupole correlation emerges from the coupling of these two orbitals from both valence neutrons and protons outside the ^{100}Sn core [1].

In this region, the octupole band is known for a few cases and only for ^{114}Xe the reduced transition probability for the octupolar electric transition B(E3: $3^- \rightarrow 0^+$) has been measured to be 70 W.u., resulting in one of the largest octupole strengths ever measured [3]. Indeed the value of this observable, proportional to the E3 transition rate between the 3^- and 0^+ states, represents a measure of the octupolar deformation strength.

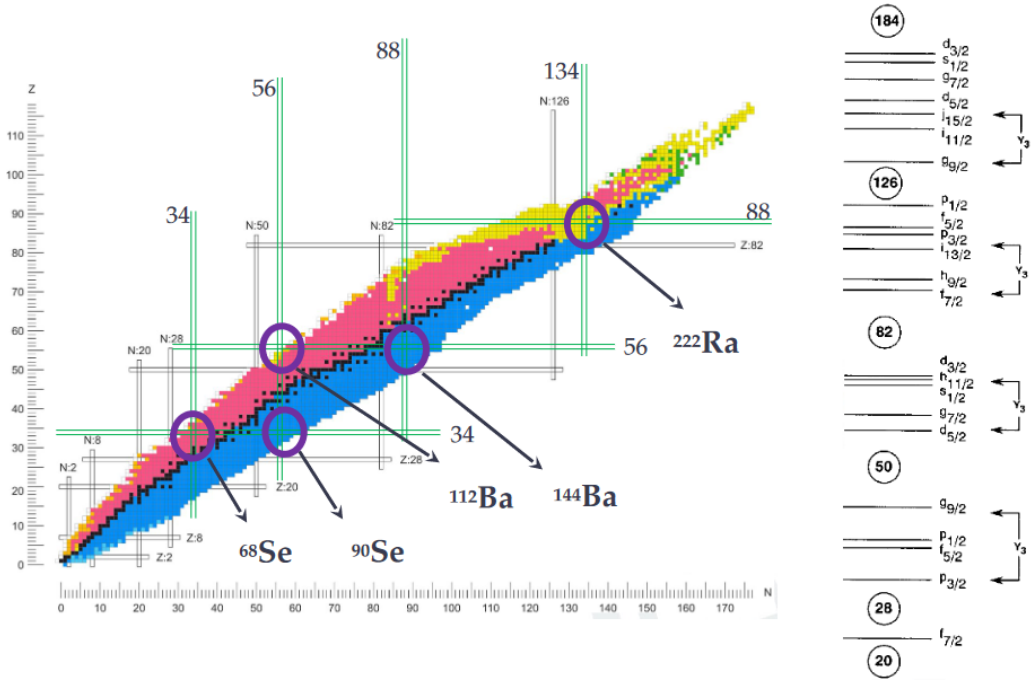

Figure 2: The Segré chart (left), where the violet circles represent the regions where octupole correlations are expected to be enhanced. Shell model orbitals are represented on the right side; in this case the arrows indicate the orbitals coupling which produce octupole correlations. Adapted from [1].

In the N $\simeq$ Z = 54 mass region octupole correlations are expected to be strongly enhanced. Therefore, the identification of octupole structures for more neutron deficient systems is of utmost importance to benchmark our best nuclear models. For example, as shown in Fig. 3, the maximum of B(E3: $3^- \rightarrow 0^+$) in the Xe isotopic chain is expected to occur in the neutron deficient ^{110}Xe [4].

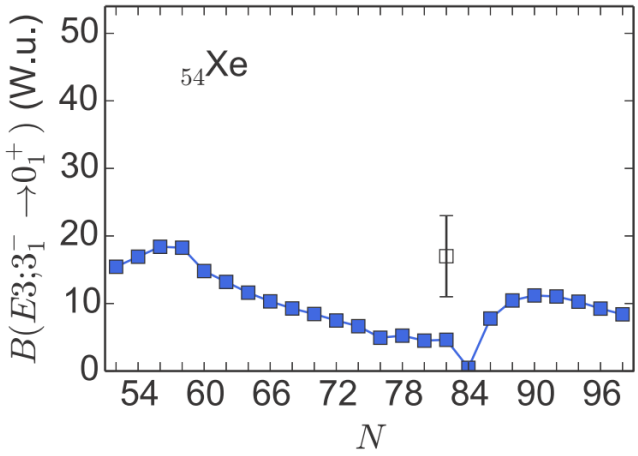

Figure 3: B(E3: $3^- \rightarrow 0^+$) reduced transition probabilities for the Xe isotopes, from [4]. Solid squares connected by lines denote the theoretical results, while the open square represents the experimental value.

This thesis presents the study of octupole correlations in the very exotic N = Z+2, N = 56, ^{110}Xe. This nucleus has been previously produced using fusion evaporation reactions [5, 6]. The cross-section was determined to be between 50 to 300 nb. To measure the excited states of ^{110}Xe with such small cross-section, it is required an highly efficient and selective detection system, which was achieved with the combination of the MARA recoil separator [7] and its focal plane detectors. Before to this study, only the ground state band of ^{110}Xe was known up to the 6^+ state [5].

Theoretical beyond mean field calculations have been performed to obtain some initial predictions for the octupole correlations in ^{110}Xe [8]. Fig. 4 shows the collective wave functions up to spin J = 10 and 9. The nature of the excited states in the positive and negative parity band can be deduced from this figure. In both cases the expected quadrupole deformation is around $\beta_2 \approx 0.2$. In the ground state band, β_3 is close to zero at low angular momentum but interestingly deviates from zero already at spin J = 8, where two symmetrical minima start to develop. The excited negative parity band shows two symmetrical well-developed minima in β_3 which appear extremely stable at increasing angular momentum. Therefore, the theoretical calculations predict an octupole band structure, similar to the one in ^{112}Xe, and confirm that the ground state band in ^{110}Xe is deformed.

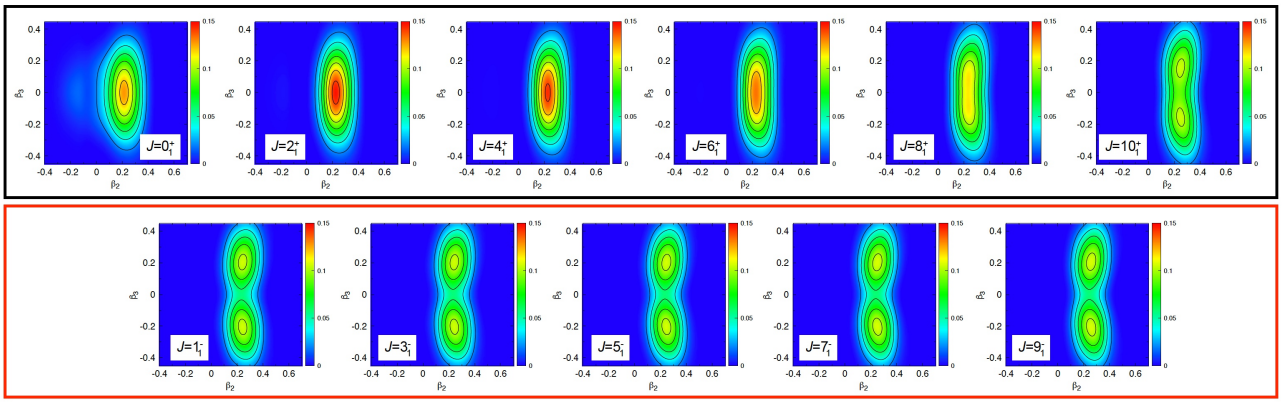

Figure 4: Collective wave functions for the ground state band (upper part) and first excited negative-parity (lower part) bands for ^{110}Xe [9].

1.2 Reaction mechanism

Fusion evaporation reactions are perfectly suited to study neutron-deficient nuclei. Indeed, fusing a system of two stable nuclei X and Y usually results in the production of a neutron-deficient compound nucleus W. In fact, since the nuclear stability line falls below the Z=N line, the $N_W/A_W=(N_X+N_Y)/(A_X+A_Y)$ ratio is much lower for these products than for stable nuclei with mass A_W.

After the two nuclei fuse, the highly-excited compound nucleus undergoes particle (proton, neutron, etc.) evaporation around 10^{-21}s after the formation. Subsequently, when the threshold of particle emission is reached, γ-ray decay dominates the decay mode at about 10^{-13}s from the formation of the compound nucleus (see Fig. 5). These γ rays are emitted in a continuum spectrum range due to the high density of states of their origin. Once the evaporation residues reach the yrast line, γ rays are emitted in a cascade from discrete energy states.

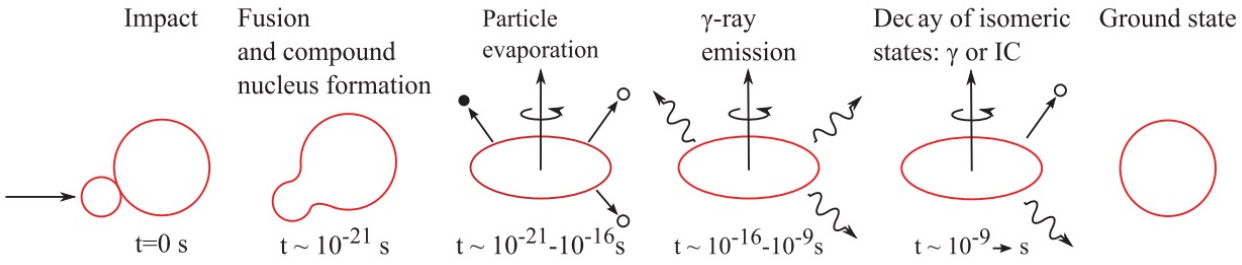

Figure 5: Schematic illustration of the fusion-evaporation reaction evolution with time, from [10].

2 Experimental setup

The experiment was carried out at the accelerator laboratory of the University of Jyväskylä (Finland) in 2020. In this experiment, a beam of ^{58}Ni at 228 MeV, with an average intensity of 3.5 pnA, impinged on a double-layer target: 1.0 mg/cm^2 of ^{197}Au and 0.75 mg/cm^2 of ^{54}Fe. The Gold layer was facing the beam to reduce the spattering of the Fe layer, caused by beam current and temperature. The compound nucleus for this reaction was ^{112}Xe. After this stage, the ^{110}Xe was produced via the evaporation of 2 neutrons.

The experimental apparatus used for this experiment consists in three main elements, as it is illustrated in Fig. 6: the High Purity Germanium detector Jurogam III [11], the recoil separator MARA [7] and its focal plane detectors [7].

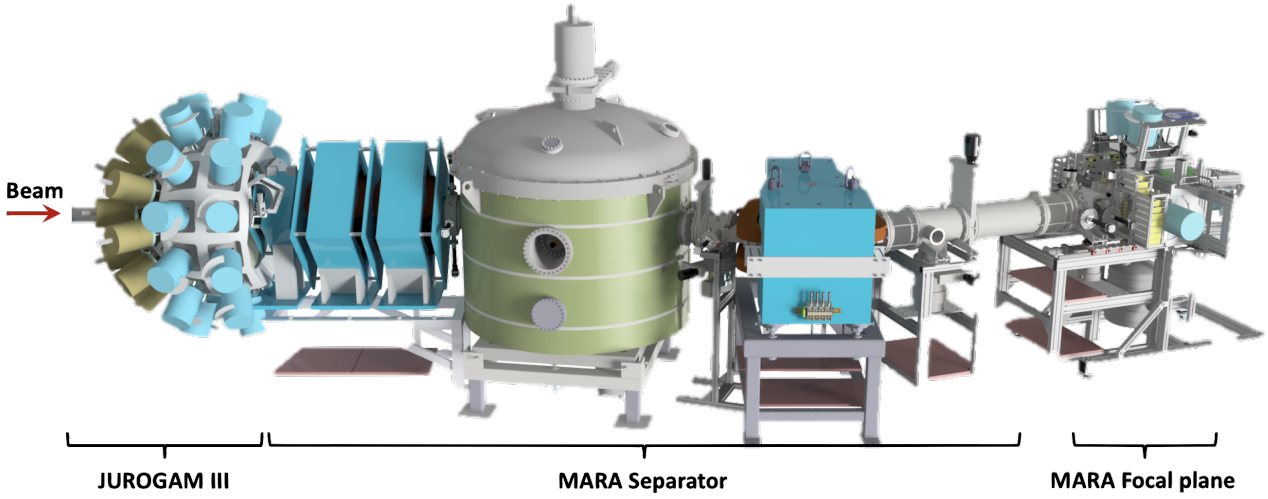

Figure 6: Schematic illustration of the experimental apparatus employed in this experiment.

2.1 JUROGAM III

Prompt γ rays emitted from excited energy states were detected by an array of High Purity Germanium (HPGe) detectors called the Jurogam III γ-ray spectrometer [11]. The array was placed at the target position upstream of the recoil separator. The Jurogam III detector consists of fifteen EUROBALL phase one [12] germanium detectors and twenty-four EUROBALL Clover detectors [13] arranged in four rings around the target chamber. The former detectors were positioned at 157.6^o and 133.57^o, while the latter ones were arranged at 104.5^o and 75.5^o. The Clover detectors have four crystals, coupled in two sub-rings at 109^o and 100^o for the first group of 12 clovers and at 80^o and 71^o for the second group. All the Germanium detectors were surrounded by anti-Compton Bismuth Germanium Oxide (BGO) shields. These BGO shieldings acted as anti-coincidence detectors to improve the peak-to-background ratio of the γ-ray spectra. The signals in the Germanium detectors were vetoed if they were detected in coincidence with a signal in the BGOs, since it could have originated from Compton scattering events, resulting in incomplete energy collection in the Germanium crystals.

2.2 MARA

The main purpose of MARA is to separate the desired nuclei from the scattered beam and the vast plethora of recoils produced by the reaction between beam and target. This is done by taking advantage of certain properties of the motion of a charged particle in the presence of an electric or magnetic field, described by the Lorentz force:

$$\vec{F} = q(\vec{E} + \vec{v} \times \vec{B}).$$

The separator consists of three main parts: a quadrupole triplet followed by an electrostatic deflector and a magnetic dipole. The role of the quadrupole triplet is to focus divergent products from the target position spatially to an area as small as possible in both directions at the focal plane. Additionally, the triplet focuses ions from point to parallel to the entrance of the dipole.

2.3 MARA Focal Plane detectors

The MARA Focal plane consists on a combination of a Multi-Wire Proportional Counter (MWPC) followed by a Double-sided Silicon Strip Detector (DSSD), where the ions are implanted. In addition, there is a broad set of complementary detectors used for measuring the decay of delayed implanted ions, such as a second DSSD punch through detector, an array of HPGe detector for γ ray measurement and a β scintillator, among others.

Multi-Wire Proportional Counter (MWPC)

The MWPC is a gas-filled proportional counter where a constant electric field is used to drive the electrons created by the passage of a heavy charged particle through matter towards electrodes for collection. The amplitude of the observed signal is directly proportional to the number of electrons produced in the interaction and independent of the voltage driving them, providing that is high enough to prevent the recombination.
In this experiment the MWPC faced the MARA separator and consisted of two planes of thin wires, 2-3 mm apart, spaced at regular intervals. The chamber was filled with low pressure gas with a low ionisation energy (isobuthane), and the charge produced when a particle passes through was collected by the wires closest to the ionisation path. This allows two-dimensional spatial information to be inferred from the position of the wires collecting charge pulses. Hence, the grid provided the position and time-stamp of the recoils impact.

2.3.1 Double-Sided Silicon Strip Detectors (DSSD)

After passing through the MWPC, the ions were implanted in a DSSD. The DSSD is a semiconductor detector capable to collect information from both sides. Indeed, the DSSD has strips on the surface of the silicon running top to bottom on one side and left to right on the other. The grid pattern allows each side of the detector to collect charge in the two strips closest to the origin of the charge carriers. The top to bottom running wires give information on where the origin of the charge is on the horizontal x axis, and the left to right wires give information on the y position, along with energy and time coordinate of the incident radiation. The DSSD mounted for this experiment was the BB20 model from Microm [14]. It consisted of 192 vertical strips on one face and 72 on the horizontal side, with a nominal thickness of 300 μm.

2.3.2 Complementary detectors

The instrumentation at MARA focal plane was completed with a β-plastic scintillator [15] placed after the DSSD and an array of three BeGe γ-ray detectors, which surrounded the DSSD and the β-plastic scintillator, employed to further determine the physical event.

2.4 DAQ system: the Total Data Readout (TDR) method

For what concerns the Data AcQuisition (DAQ) system, it was employed the Total Data Readout method. It consists in a triggerless DAQ system where all the electronics channels operate individually in free running singles mode. The TDR system allowed us to overcome dead-time limitations and to record the data stream using a 100 MHz clock signal by the metronome and channel number without using a trigger [16]. The system also included an event builder software, called TDREB [16].

In the case of an event detected at the DSSD of the MARA focal plane, a coincidence window of 10 μs was opened in order to acquire all the information in all the detectors. The size of the window depends on the time of flight of the recoils between the target and the DSSD. For this experiment, it starts 2.0 μs before the trigger signal in the DSSD y side.

3 Data analysis

3.1 Calibration of Jurogam III

For a correct and precise analysis of the γ-ray spectra the energy and efficiency calibration of the detectors is essential. In this experiment radioactive sources of ^{152}Eu and ^{133}Ba were used both for energy and efficiency calibrations of Jurogam III, as discussed in the following section.

3.1.1 Energy calibration

The ^{152}Eu and ^{133}Ba radioactive sources were placed at the center of the γ-ray array. Gamma-ray transitions were selected in the range 80-1408 keV and the energy was calibrated as a function of channel number using the equation

$$E = a + (ch \cdot b) + (ch^2 \cdot c), \tag{2}$$

where ch is the channel number and a, b and c are the offset, the linear and the quadratic term coefficients, respectively.

3.1.2 Efficiency calibration

Gamma-ray detectors efficiency has a strong dependence on the energy of the detected γ ray. In order to build up a level scheme, a precise knowledge of the detection efficiency is needed to extract the γ-ray intensities. The absolute photopeak efficiency at a given energy E, ϵ_{abs}(E), is defined as the ratio between the detected number of γ rays, N_D(E), and the emitted γ rays, N_E(E), from the radioactive source:

$$\epsilon_{abs}(E) = \frac{N_D(E)}{N_E(E)} \times 100. \tag{3}$$

Knowing the activity of the reference source (A_{ref}) , the duration of the measurement (Δt), and the tabulated branching ratio of the transition (I$_\gamma$(E)), the equation can be rewritten as

$$\epsilon_{abs}(E) = \frac{N_D(E)}{A_{ref} I_\gamma(E) \Delta t} \times 100. \tag{4}$$

As mentioned above, the determination of the absolute efficiency of Jurogam III was established by placing radioactive sources of ^{133}Ba and ^{152}Eu at the target position, both at the Beginning Of the Experiment (BOE) and at the End Of the Experiment (EOE). The efficiency curve used to fit the data [17] is:

$$\epsilon_{abs}(E) = exp[(A + B \cdot x + C \cdot x^2)^{-G} + (D + E \cdot y + F \cdot y^2)^{-G}]^{-1/G}, \tag{5}$$

where x = log(E/100[keV]) and y = log(E/1000[keV]). The result obtained is shown in Fig. 7.

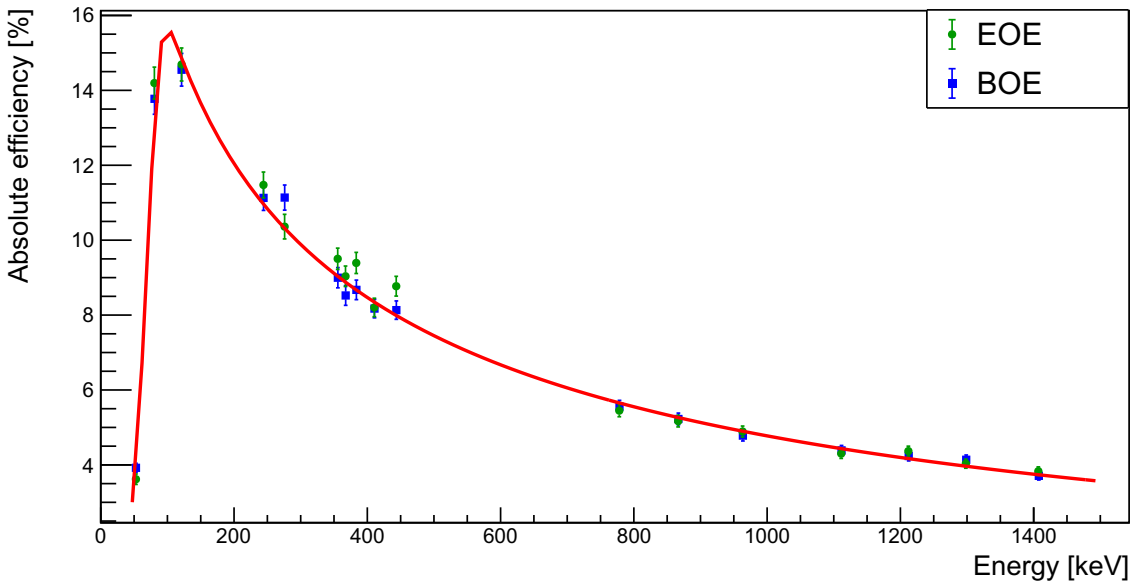

Figure 7: Absolute efficiency curve for the Jurogam III array. BOE denotes the measurements with the radioactive sources performed at the beginning of the experiment and EOE at the end of the experiment.

In order to perform an angular distribution analysis of the transitions under study (see Section 4.4), the efficiency curves for each ring were needed. The fits obtained are shown in Fig. 8.

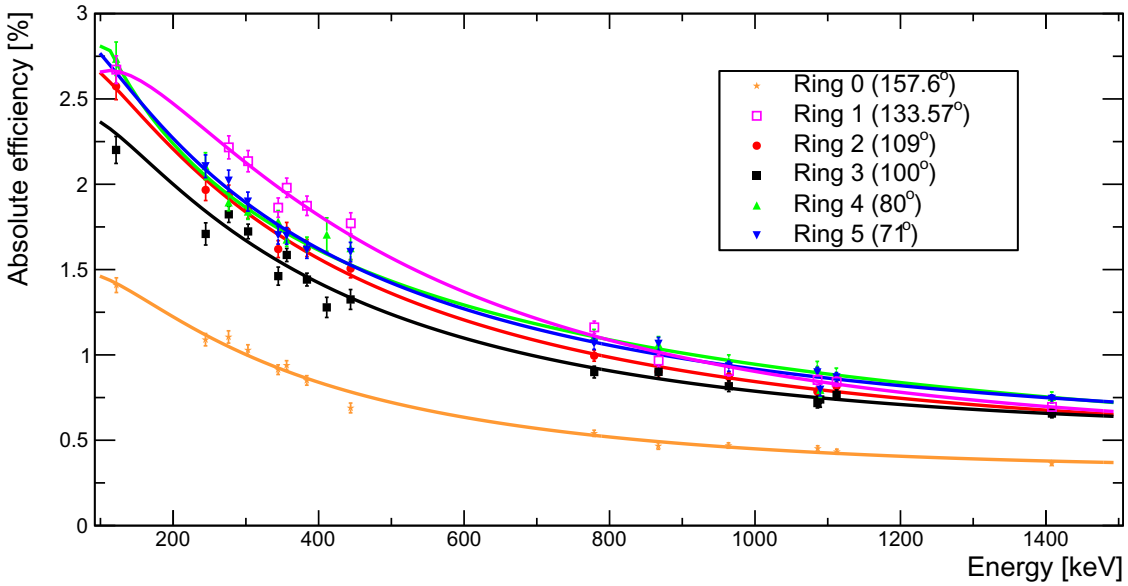

Figure 8: Absolute efficiency curve ring by ring for Jurogam III for this experiment.

3.2 Selection of the recoils of interest

The first step consisted in the discrimination between the beam particles, target particles and fusion-evaporation recoils arriving at the focal plane. For that, the time of flight from the signal in the MWPC and the implantation into the DSSD was recorded and analysed. After this stage, the MARA separator was used to split different mass over charge (A/q) states of the recoils. In particular, the electrostatic deflector separated nuclides by their energy and the magnetic dipole splitted each charge state according to their momentum. Finally, the spectra were cleaned up with the Recoil Decay Tagging (RDT) method.

3.2.1 The Recoil Decay Tagging (RDT) Technique

As previously stated, the compound system in a fusion-evaporation reaction can evaporate many different combinations of protons, neutrons and α particles, resulting in a large amount of reaction channels. As a result, a highly efficient and selective detection system is necessary to distinguish between different channels. In this experiment the required selectivity was achieved using the Recoil-Decay Tagging (RDT) method [18]. This method relies on the decay properties (α, β, proton, etc) of each recoil for their identification, allowing us to tag the prompt γ-ray transitions.

In particular, in the region of the Segré Chart under study the isotopes decay primarily in the α channel, allowing the very selective α-tagging method to be employed. In this experiment the α decays following the implantation of the recoils in the DSSD were correlated to the events recorded in Jurogam III and in the MWPC. In particular, conditions on the time and energy of the decay were applied in order to select the prompt γ transitions of the fusion-evaporation residues of interest. From [19] is known that ^{110}Xe decays α to ^{106}Te with a branching ratio of (64±35)%. Furthermore, ^{106}Te undergoes α decay with a branching ratio of 100% [19]. Thus, in this case it was possible to employ the $\alpha\alpha$ tagging technique, requiring a time limit of 500 μs and 35 μs after the previous event in the same DSSD pixel and the α energy in the interval 3.5-4 MeV and 3.95-4.25 MeV for the first and the second alpha decay, respectively. Fig. 9 shows the spectra obtained gating with only one or the two successive α decays. One can see how the γ-ray spectrum is clean, and we can confirm that all the lines identified belong to ^{110}Xe.

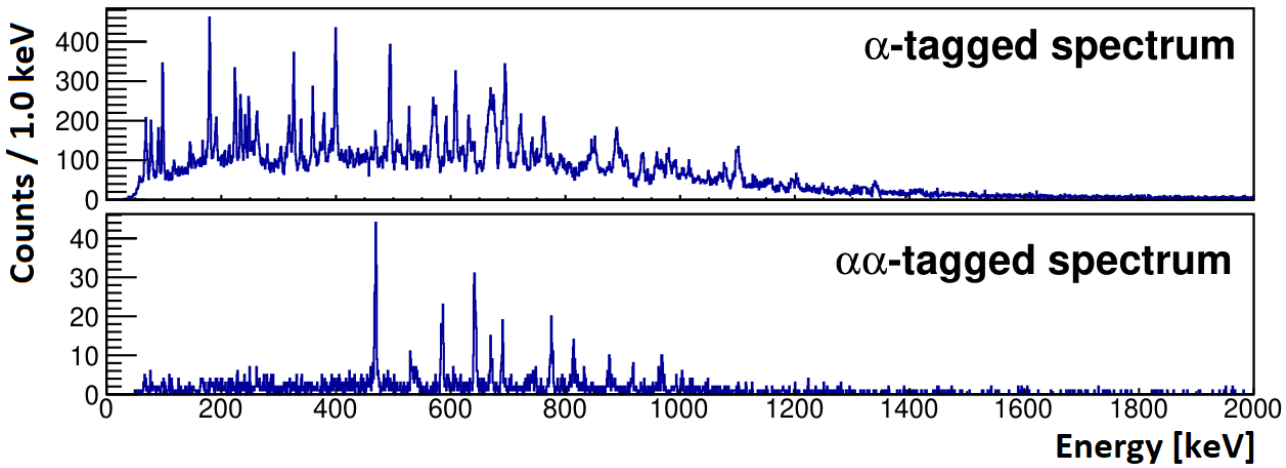

Figure 9: Recoil-decay tagging spectra: spectrum obtained gating only on the first α decay (top) and both on the first and the second (bottom).

3.3 Gamma Doppler correction

Gamma rays emitted by nuclei in movement are affected by the Doppler effect. The observed energy of a photon emitted by a moving nucleus is given by

$$E'_\gamma = E_\gamma \frac{\sqrt{1-\beta^2}}{1-\beta cos(\theta)} \tag{6}$$

where E_γ is the energy of the photon emitted at rest, $\beta = v/c$ is the modulus of the nucleus velocity and θ is the angle between the velocity vector of the nucleus and the direction of the emitted gamma ray. In order to obtain the correct energies for these transitions, the γ rays detected in each ring need to be Doppler corrected.

In the reaction under study, since the evaporated particle (neutrons) have negligible masses if compared to the Xe nucleus, from momentum conservation we can consider the direction of the recoils to be the same as the beam. Therefore, the angle θ can be approximated as the angle of the detectors with respect to the beam axis.

In this experiment, the β values were derived performing a least-squares fit of the Doppler-shifted energy as a function of the ring angle θ. For each nucleus, we performed the fit for the most intense γ-ray transitions and the average of the different β values obtained was used for the Doppler correction. Fig. 10 shows the least-squares fits for the energy of two of the most intense γ-ray transitions of ^{109}Te spectrum, respectively at 609 keV and 695 keV, as a function of θ.

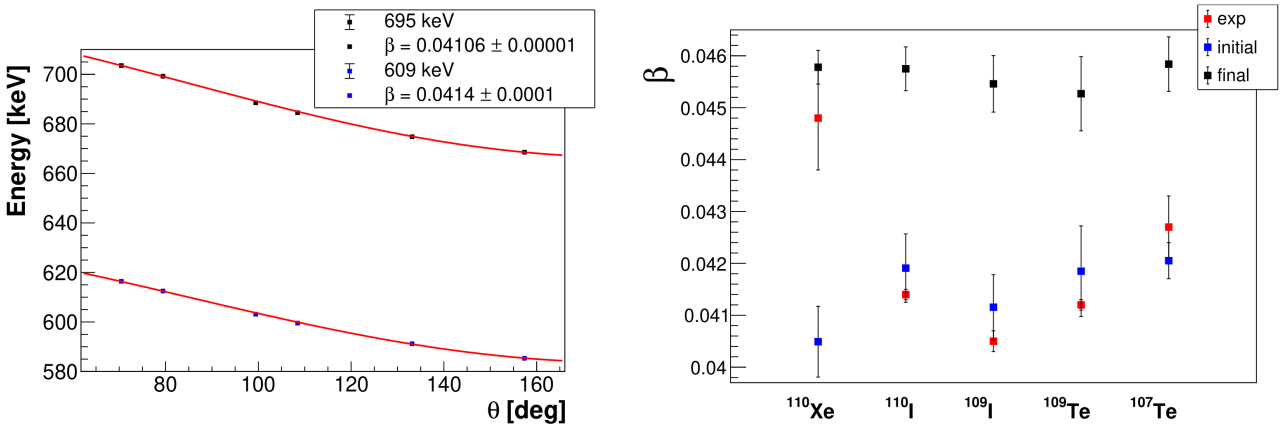

Figure 10: On the left: fit of the Doppler-shift energy as a function of the ring angle for the most intense peaks of ^{109}Te spectrum, namely 609 keV and 695 keV. Given the high statistics, the relative errors for the energies are of the order of 0.1%. On the right: velocities for the reactions products identified in this experiment. The experimental values are marked in red, while the ones calculated with PACE4 are indicated in blue and black. They correspond to the reaction taking place at the beginning (blue) and at the end of the target (black).

We calculated the expected velocities with PACE4 [20, 21]. The calculations were performed taking into account two limits: the reaction taking place at the beginning or at the end of the ^{54}Fe layer of the target. The latter case was indicated as "final" in Fig. 10, while the former, where the energy loss of the recoils was taken into account, was labelled as "initial". In both cases the presence of ^{197}Au layer was considered. It can be observed how the velocities calculated for the reaction taking place at the beginning of the target agree, within the errors, with the experimental values, labeled as "exp" in the figure. In the case of ^{110}Xe, given the low statistics the centroids of the peaks present large uncertainties. As a result, the experimental value of β considerably differs from the one calculated for the reaction at the beginning of the target and from the values obtained for ^{110}I, ^{109}I, ^{109}Te and ^{107}Te.

In order to obtain the optimal value for the velocity of ^{110}Xe (β_{opt}) we analysed the spectra obtained using different values of β, ranging from 0.040 to 0.045. Comparing the most intense transitions energies, we obtained the best resolution with $\beta = 0.04232$ and therefore we used this value as β_{opt}.

An example of the Doppler effect and its correction per ring of detectors is illustrated Fig. 11 using the γ-ray spectra obtained in coincidence with ^{109}Te. The energy dependency on the angle (left panel in Fig. 11) disappears after the proper Doppler correction (right panel in Fig. 11).

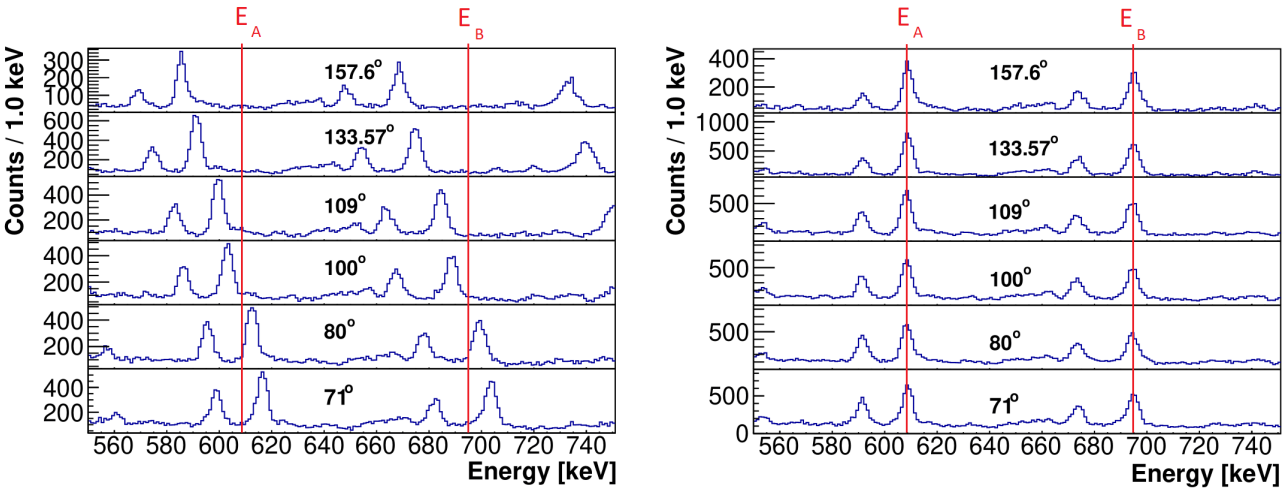

Figure 11: Non Doppler corrected (left) and Doppler corrected (right) γ-ray spectra ring by ring obtained in coincidence with ^{109}Te, in the energy range from 550 keV to 750 keV. The value of β used for the Doppler correction was β=0.0410, deduced from the fits described above.

4 Experimental results

In this section the results of the data analysis for ^{110}Xe are presented and discussed. Despite the low cross section of this reaction channel, we were able to expand the ^{110}Xe level scheme. In particular, we identified the low-lying octupole band transitions, that could not be identified in a previous study on this nucleus [5].

4.1 Gamma-ray spectrum of ^{110}Xe

The first step for building the level scheme was the identification of the γ-ray transitions and their relative intensities in the γ-ray spectrum, shown in Fig. 12.

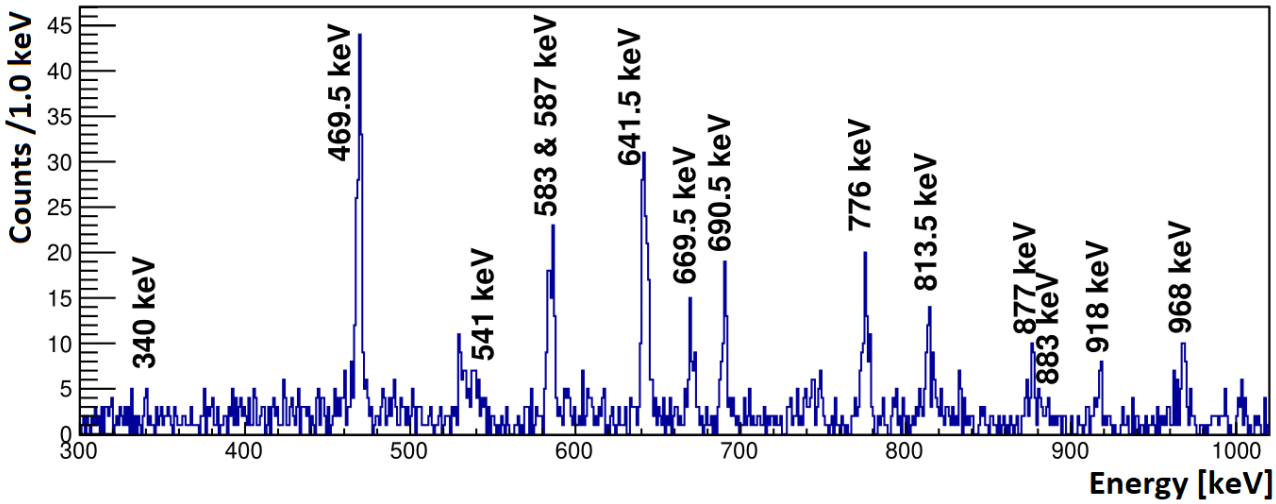

Figure 12: Spectrum of the prompt γ transitions of ^{110}Xe obtained after the $\alpha\alpha$ tagging. The energies of the γ rays included in the level scheme in Fig. 16 are reported.

The intensities I(E) of the γ-ray transitions were derived correcting the measured areas A with the absolute efficiency ϵ_{abs} at the γ-ray energy E. Eventually the intensities were normalised with the area $\tilde{A}$, corrected by efficiency, of the 469.5(1) keV γ ray, identified as the transition to the ground state:

$$I = \frac{A}{\epsilon_{abs} \cdot \tilde{A}} \times 100. \tag{7}$$

In addition, the possible decay from a state via internal conversion was taken into account. For this purpose, the contribution of this process to the total intensity has been evaluated for each state using the Conversion Coefficient Calculator [22], and resulted always lower than 2%. Table 1 lists all the transition energies and the corrected intensities obtained in this experiment for ^{110}Xe.

Table 1: Energies and intensities corrected by efficiency and internal conversion of the most intense transitions observed for ^{110}Xe.

E [keV]	**I [%]**
340.1(2)	3(3)
469.5(1)	100(17)
530.3(3)	13(6)
533.3(5)	12(6)
538.2(5)	13(6)
541.1(8)	6(4)
583.5(3)	32(10)

E [keV]	**I [%]**
586.5(3)	39(11)
641.0(2)	74(16)
644.1(3)	29(10)
669.6(2)	21(9)
672.2(3)	12(6)
690.2(2)	38(12)
775.7(3)	43(13)*

E [keV]	**I [%]**
778.3(1)	19(9)
813.6(3)	33(11)
876.9(2)	21(9)
883.5(1)	3(3)
917.7(3)	15(8)
968.3(3)	33(12)
1002.8(7)	22(10)

*The intensity of the 775.7(3) keV γ ray represents the sum of intensities of two γ transitions.

4.2 Gamma-gamma coincidence analysis

To establish the level scheme of any nucleus, it is needed to understand which transitions are in coincidence (i.e. they are part of the same decay path) and the intensity balance between the different cases. For this reason, the data were processed using a $\gamma\gamma$ coincidences matrix within a time difference constrain of the order of the intrinsic time resolution of the detector, i.e. 10 ns. By selecting several γ-ray projections on the matrix (as indicated in Fig. 13) the level scheme could be constructed.

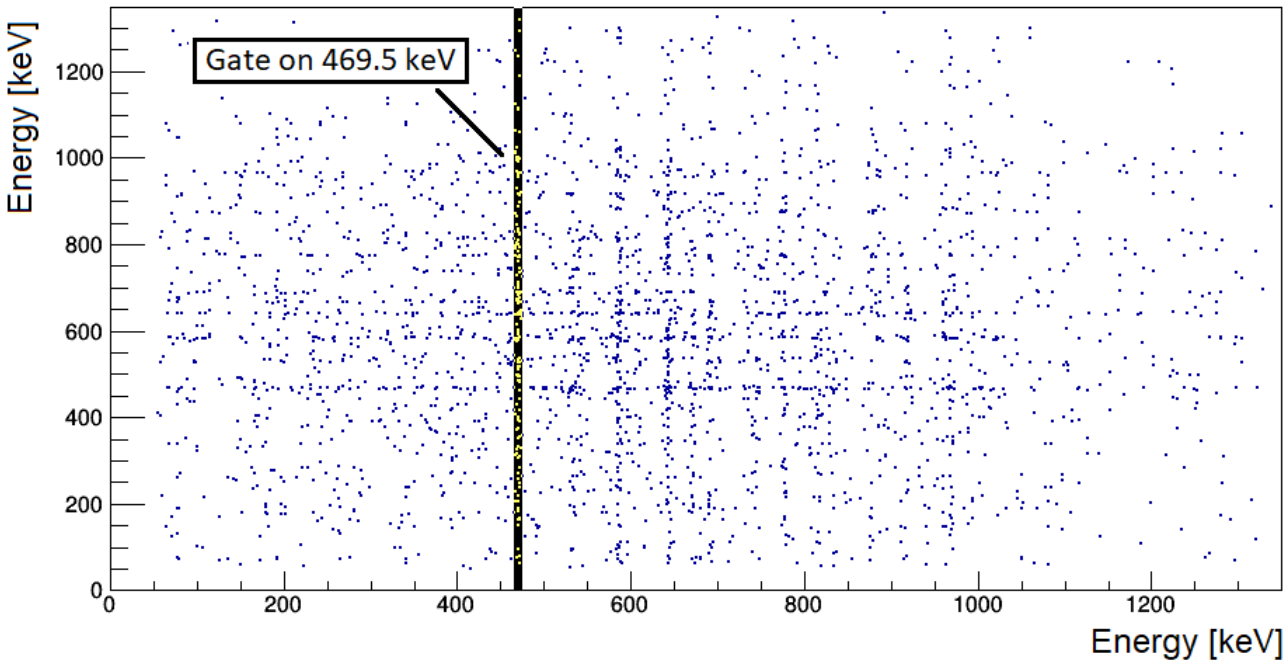

Figure 13: $\gamma\gamma$ matrix for ^{110}Xe. The highlighted region represents the energy window ΔE employed to identify the γ rays in coincidence with the most intense transition, of energy 469.5(1) keV.

The first step for building a level scheme is to determine the γ ray of the most intense transition in the γ-ray spectrum (Fig. 12), in this case 469.5(1) keV. From the systematics of the neighbouring nuclei (see Section 4.5) and considering that it is in coincidence with all the most intense γ rays (see Fig. 14 and Fig. 15), this transition was identified as the $2^+ \rightarrow 0^+$, in accordance with [5]. In the same way, the second most intense transition with an energy of 641.0(2) keV was identified as the $4^+ \rightarrow 2^+$.

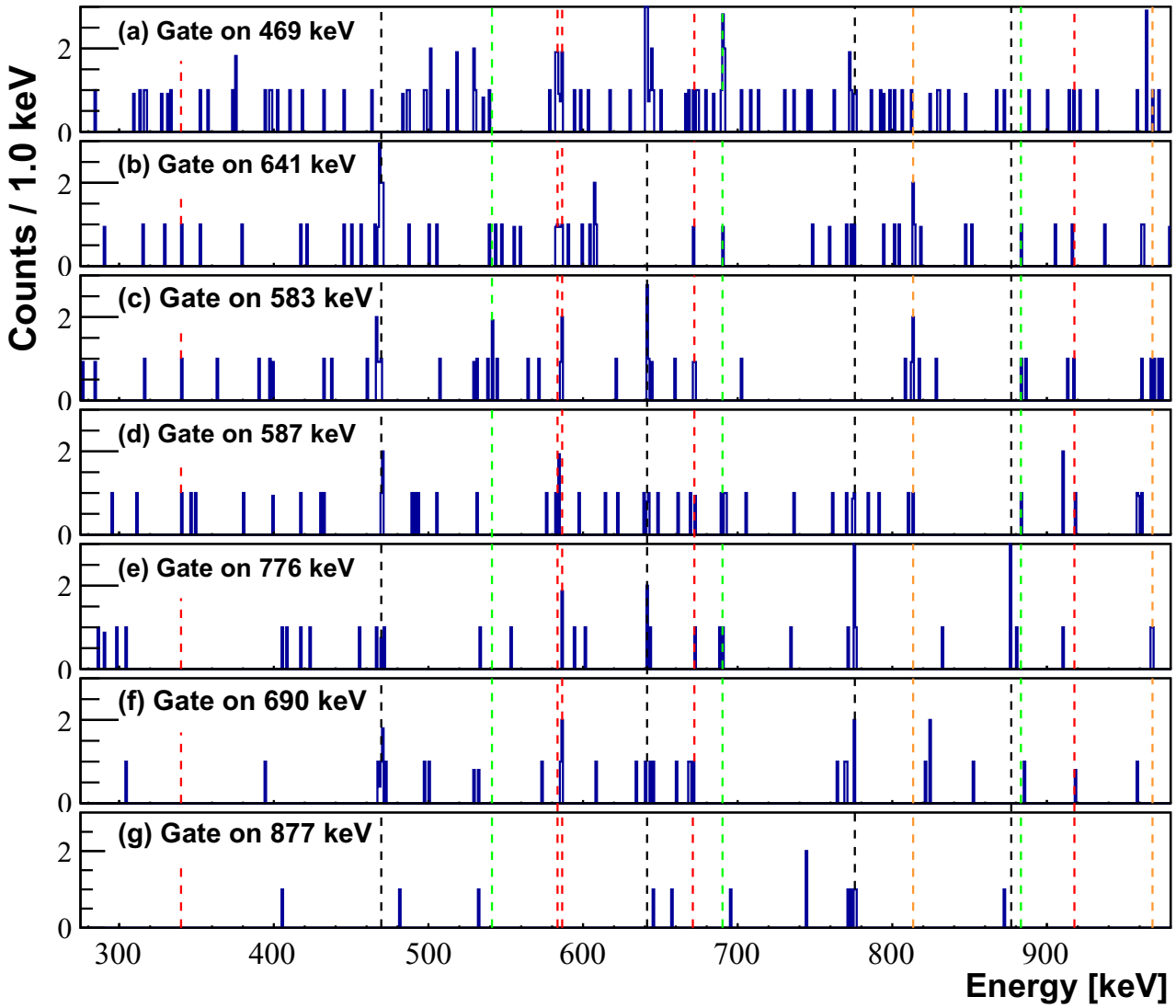

Figure 14: Spectra obtained gating on the transitions with energy of 469 keV ($2^+ \rightarrow 0^+$), 641 keV ($4^+ \rightarrow 2^+$), 583 keV ($7^- \rightarrow 5^-$), 587 keV ($9^- \rightarrow 7^-$), 776 keV ($6^+ \rightarrow 4^+$) , 690 keV ($7^- \rightarrow 6^+$) and 877 keV ($8^+ \rightarrow 6^+$). The vertical lines correspond to the energy of the transitions placed in the level scheme: in black for the γ rays belonging to the ground state band, in red for the ones of the octupole band and in green for the ones connecting the two bands. The transitions feeding the octupole band are drawn in orange.

The next step consisted in the identification of the levels lying above the 4^+ state. Except for the 469.5(1) keV and 641.0(2) keV transitions, all the remaining most intense transitions are not in coincidence, suggesting the presence of more than a single band in the level scheme. This is corroborated by the systematic of the neighbouring nuclei, where the 4^+ state is fed by two levels belonging to different bands (see Section 4.5). In order to determine the low-lying levels of the octupole band, we tried to identify the interband transitions by investigating two separate cascades, each composed by a pair of transitions:

- the $7^- \rightarrow 6^+$ de-excitation, labelled as (x), followed by the $6^+ \rightarrow 4^+$ transition, labelled as (y)
- the $7^- \rightarrow 5^-$ transition, labelled as (z), with a subsequent $5^- \rightarrow 4^+$ transition, labelled as (w).

All the possible combinations of the γ rays presented in Table 1 were tested, applying both energy balance arguments and coincidence analysis. The only two pairs of γ rays where the sum of the energies of (x) and (y), in coincidence, was equal to the sum of the energies of (z) and (w), in coincidence, corresponded to: (x)=690.2(2) keV, (y)=775.7(3) keV, (z)=583.5(3) keV and (w)=883.5(1) keV. The first pair of transitions is not in coincidence with the second one, and even exploring other possible decay paths, for example two separated cascades from the 9^- state to the 4^+ state, this remained the most convincing one.

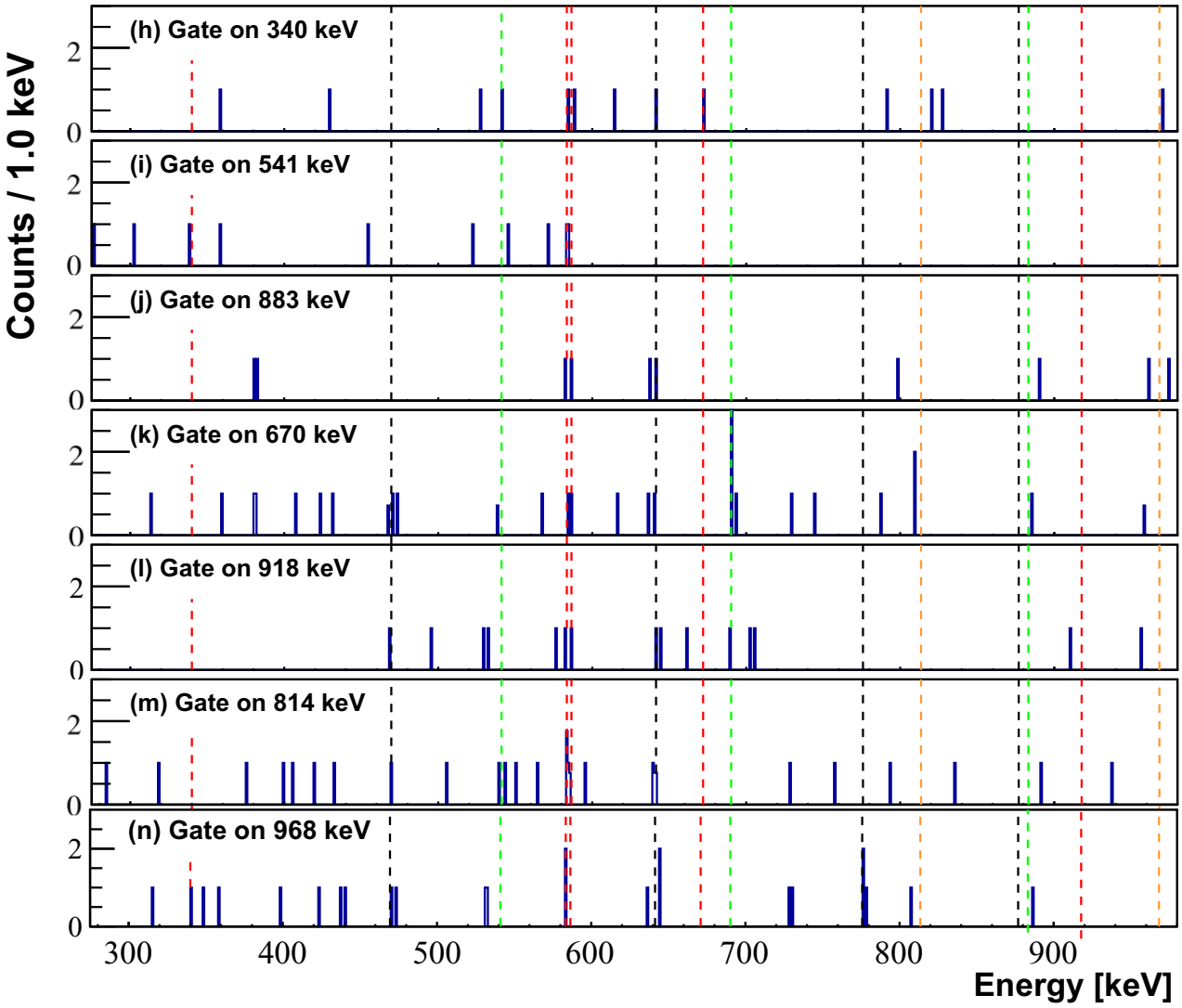

Figure 15: Spectra obtained gating on the transitions with energy of 340 keV ($5^- \rightarrow 3^-$), 541 keV ($3^- \rightarrow 4^+$), 883 keV ($5^- \rightarrow 4^+$), 670 keV ($11^- \rightarrow 9^-$), 918 keV ($13^- \rightarrow 11^-$) , 814 keV ($11^- \rightarrow 9^-$) and 968 keV ($9^- \rightarrow 7^-$). The vertical lines correspond to the energy of the transitions placed in the level scheme: in black for the γ rays belonging to the ground state band, in red for the ones of the octupole band and in green for the ones connecting the two bands. The transitions feeding the octupole band are drawn in orange.

Having established the energy of the 7^- state, the next step was to determine the levels lying above it. The only γ ray not placed in the level scheme yet and in coincidence with all the others previously mentioned is the 586.5(3) keV one. According to the systematics of ^{112}Xe and ^{114}Xe, we identified it as the $9^- \rightarrow 7^-$ transition. For what concerns the remaining transitions, they are not in coincidence with all the transitions discussed so far. We calculated the probability for this to happen: given the low statistics available, we treated the detection of a γ as a binomial event with a probability p to occur equal to the efficiency $\epsilon(E)$ of Jurogam III at the energy of the γ transition.

Considering N counts with energy E_1 in the spectrum in singles (Fig. 12) and gating on it, the probability to observe zero coincidence events with a second γ of energy E_2 is equal to

$$P(0) = (1-p)^N = (1-\epsilon(E_2))^N. \quad (8)$$

Gating on each transition not placed in the level scheme, the probability P(0) to see zero coincidences with every other γ ray already identified is always greater than 30%. The only exception is between 641.0(2) keV and 968.3(3) keV, where we still have a non-negligible probability of 14%. We identified four γ rays, with energy 669.6(2) keV, 917.7(3) keV, 813.6(3) keV and 968.3(3) keV, in coincidence with at least two of the transitions already placed in the level scheme. These four are not in coincidence with one another, as a possible evidence for them to be part of different cascades. On the other hand, looking at ^{112}Xe and ^{114}Xe, and considering that the intensities of the 669.6(2) keV and 917.7(3) keV γ rays are much lower than the other two, we tentatively assigned them as the $11^- \rightarrow 9^-$ and $13^- \rightarrow 11^-$ transitions, even if they are not in coincidence. However, if we assume that they belong to the same cascade, the probability to see zero counts at 669.6(2) keV when gating in the 917.7(3) keV transition (N1=14 counts) is $P(0) = (1-\epsilon(669.6))^{N1} = (1-0.0634)^{14} \simeq 40\%$, compatible with the observations.

For what concerns the 813.6(3) keV and 968.3(3) keV γ rays, both their placement and the spin and parity (J^π) assignment of the corresponding levels descend from $\gamma\gamma$ coincidence analysis and are corroborated by previous studies on ^{112}Xe and ^{114}Xe [23, 3]. In particular, it should be underlined the coincidence of both γ rays with the 583.5(3) keV transition, while only the 813.6(3) keV γ transition is present in the 586.5(3) keV gated spectrum.

Regarding the identification of the levels above the 6^+ state in the ground state band, the γ ray at 775.7 (3) keV was observed in coincidence with the 876.9(2) keV transition and a γ ray with the same energy. Since it was not possible to disentangle the two transitions with the same energy, comparing these data with the energies and intensities in the ground state band of ^{112}Xe [23], we identified the 876.9(2) keV and second transition with energy 775.7(3) keV γ as the $8^+ \rightarrow 6^+$ and $10^+ \rightarrow 8^+$ transitions, respectively. For the same reason, in the level scheme of Fig. 16, the intensity of the latter was assumed negligible if compared to the $6^+ \rightarrow 4^+$ γ ray. Indeed the $6^+ \rightarrow 4^+$ transition should have an intensity at least equal to the one of 690.2(2) keV, since this constitutes a feeding to the 6^+ state. The fact that the 876.9(2) keV γ ray is not in coincidence with both the 469.5(1) keV and 641.0(2) keV transitions is compatible with the low statistics available. Indeed, in these cases the probability of having zero coincidences when gating on the 876.9(2) keV γ ray is higher than 19%.

An attempt was made to identify additional levels lying above the 10^+ and 13^- states, summing all the spectra gated respectively on the ground state and octupole band transitions, but because of the low statistics we were not able to identify more new levels. At last, in order to justify the intensity imbalance between the $7^- \rightarrow 5^-$ and $5^- \rightarrow 4^+$ transitions, we identified a cascade of two γ rays connecting the 5^- and 4^+ states: the two transitions with energies 340.1(2) keV and 541.1(8) keV are compatible with the energy balance and in coincidence exclusively with the γ rays of the octupole band. Looking at the systematics Fig. 20 we tentatively identified them with the $5^- \rightarrow 3^-$ and $3^- \rightarrow 4^+$ transitions, respectively.

4.3 Level scheme of ^{110}Xe

From the analysis of the coincidence relationships between the most intense transitions observed, along with comparisons with the systematics of the neighbouring nuclei and energy and intensity balance arguments, we were able to extend the level scheme of ^{110}Xe. The results are presented in Fig. 16 b), together with the level scheme obtained in the previous work on ^{110}Xe [5] a). The energies of the 2^+, 4^+ and 6^+ agree within the errors, except for the $4^+ \rightarrow 2^+$ transition.

Indeed in this case we propose a doublet of transitions with roughly the same energy, which was not possible to observe in [5] because of the lower statistics obtained.

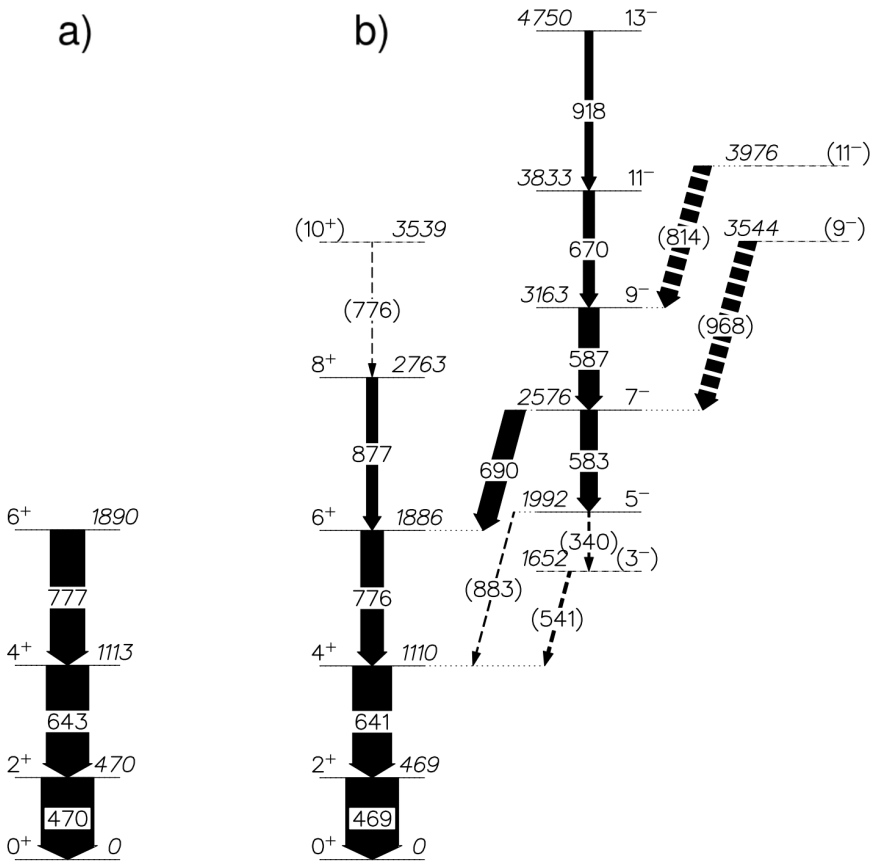

Figure 16: a) Level scheme obtained in the previous work on ^{110}Xe [5]. b) Level scheme deduced in this work. The widths of the arrows correspond to the relative intensities of γ-ray transitions. Dashed lines represent tentative levels and transitions.

4.4 Angular distributions

To assign the spin and parity to the energy levels identified, and therefore to validate the new level scheme, the type of multipolarity for each transition should be investigated. In γ decays the angular momentum and the parity of the system is conserved; if we indicate with J_i and J_f the angular momentum of the initial and final states, the angular momentum L carried by the γ ray has to satisfy the equation

$$||J_i - J_f|| \leq L \leq J_i + J_f, \tag{9}$$

while the change in parity is given by $\Delta\pi(\mathrm{EL}) = (\text{-}1)^L$ and $\Delta\pi(\mathrm{ML}) = (\text{-}1)^{L+1}$ for γ rays of electric (EL) and magnetic (ML) character, respectively [24]. The value of L characterizes the multipolarity of the transitions: one can have dipole (L=1), quadrupole (L=2), octupole (L=3) etc. transitions.

In fusion-evaporation reactions the compound nucleus is typically formed in a state with the angular momentum vector perpendicular to the axis defined by the direction of the beam. The subsequent evaporation of particles causes some smearing of the direction of the 'polarisation', but even so the nucleus retains a high degree of orientation. When a nucleus in such a state emits γ radiation, the relative intensities at different angles with respect to the beam axis depend on the multipolarity of the transition.

In general, the γ-ray intensity distributions at a given angle θ to the beam direction [25] are given by

$$I(\theta) = \sum_{l=even} a_l P_l(cos(\theta)) \tag{10}$$

where a_l are the angular distribution coefficients of the Legendre polynomials $P_l(\cos(\theta))$ [26, 24].

Looking at the systematics of the neighbouring nuclei [23, 3], the nature of the transitions between levels of the same bands is expected to be E2, while the most intense interband ones should be E1. Therefore, studying the angular distribution of the most intense transitions for ^{110}Xe can validate the level scheme proposed in this thesis.

We verified the angular distribution for ΔL=1 and ΔL=2 for ^{109}Te, that is the nucleus produced with the highest statistics in this experiment. The multipolarity of these transitions was previously established [27]. In particular the γ rays of energy 695 keV and 609 keV are expected to show an E2 behaviour, while the 317 keV and 326 keV ones should be E1. The number of counts for each peak as a function of the angle of the Jurogam III ring with respect to the beam axis is shown in Fig. 17. The angular distribution was fitted with the equation

$$I(\theta) = a_0(P_0(cos(\theta)) + a_1 P_1(cos(\theta))) = a_0(1 + \frac{a_1}{2}(3cos^2(\theta) - 1)), \tag{11}$$

with a_0 and a_1 as free parameters. A normalisation factor was included in a_0, so as to have a probability distribution.

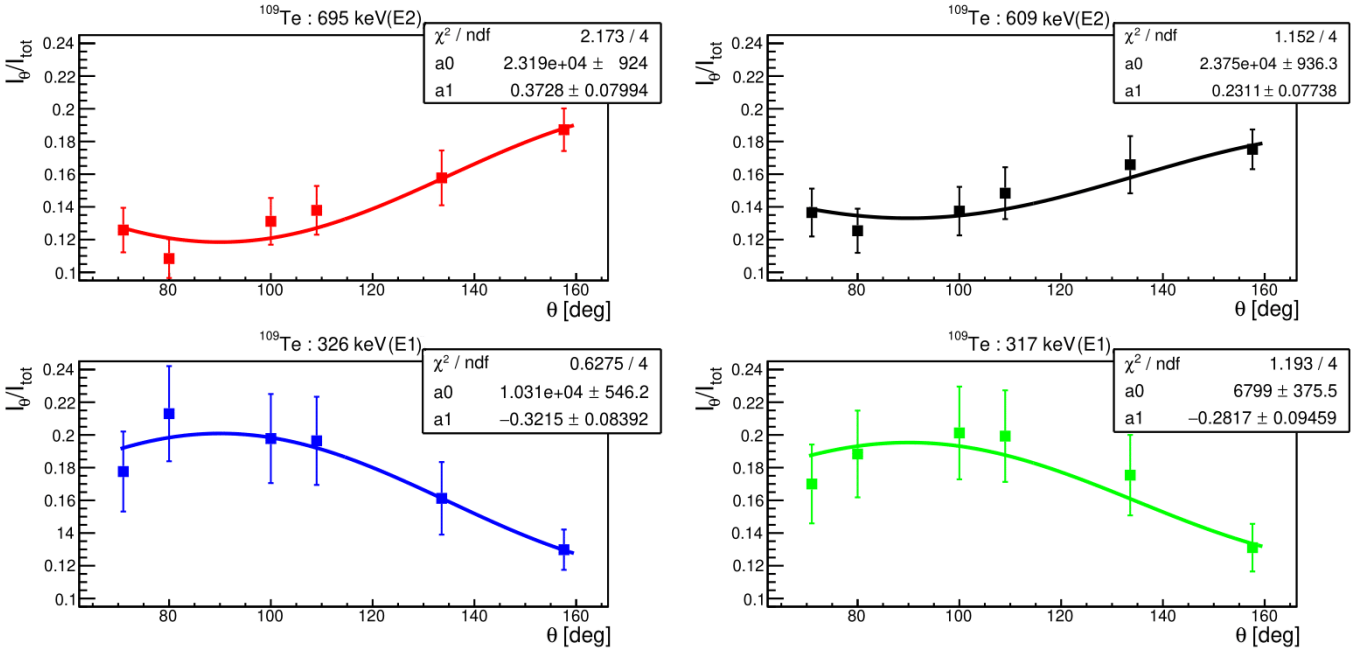

Figure 17: Angular distribution of four γ rays emitted by ^{109}Te: two E2 transitions with energy 695 keV and 609 keV (top panels) and two E1 transitions with energy 326 keV and 317 keV (bottom panels).

The value of a_1 is expected to be negative for ΔL=1 and positive for ΔL=2 [24]. Fig. 17 shows the angular distribution for ^{109}Te transitions. It confirms the character of the analysed γ rays and the fact that we are sensible to measure the multipolarity of the transitions. Since the ^{110}Xe presents very low statistics in each ring, we were able to investigate only two cases, presented in Fig. 18:

- the sum of 583.5(3) keV and 586.5(3) keV transitions, which we propose to be ΔL=2
- the 690.2(2) keV transition, which we proposed to be ΔL=1.

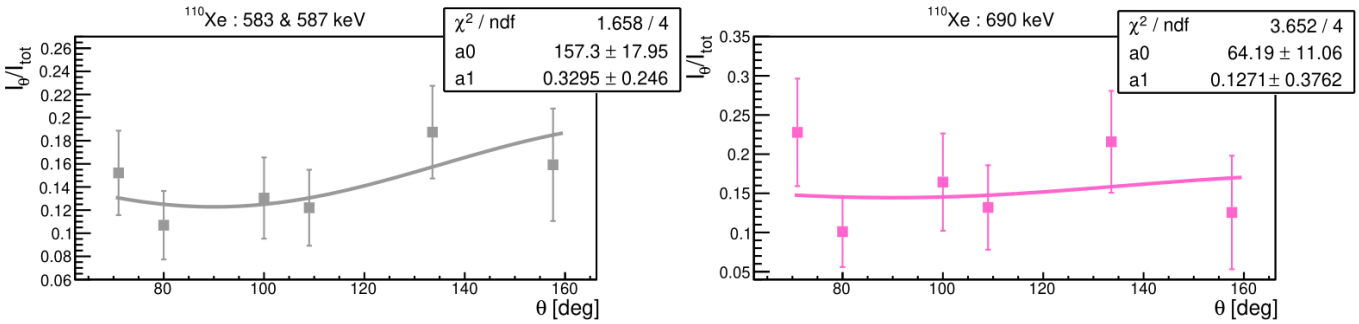

Figure 18: Angular distribution of γ rays emitted by ^{110}Xe: the sum of two transitions with energy 583.5(3) keV and 586.5(3) keV, which we propose to be ΔL=2 (on the left), and another γ ray we propose to be ΔL=1 with energy 690.2(2) keV (on the right).

The 583.5(3) keV and 586.5(3) keV transitions agree with ΔL=2 transitions, while no conclusions can be drawn about the nature of the 690.2(2) keV γ ray, since the relative error on a_1 is roughly 300%. However, we cannot reach definitive conclusions for ^{110}Xe due to the low statistics available.

4.5 Systematics with the neighbouring nuclei

The ^{110}Xe nucleus is expected to show similar characteristics to its neighbouring even-even Xenon isotopes, namely ^{112}Xe [23] and ^{114}Xe [3]. Fig. 19 shows the corresponding level schemes, where the presence of the low-lying negative parity band is a clear evidence of enhanced octupole correlations. However, a significant difference stands out: as the number N of neutrons increases the most intense interband transition occurs at lower J^π. In particular, for ^{110}Xe the most intense interband transition connects the 7^- and 6^+ states, for ^{112}Xe the 5^- and 4^+, while in ^{114}Xe it constitutes the decay from the 3^- to the 2^+ state. In addition, for ^{114}Xe a strong $3^- \rightarrow 0^+$ transition was observed, meanwhile this transition was not observed neither in ^{112}Xe [23] nor in this work for ^{110}Xe. However, due to the low statistics we cannot rule out its existence.

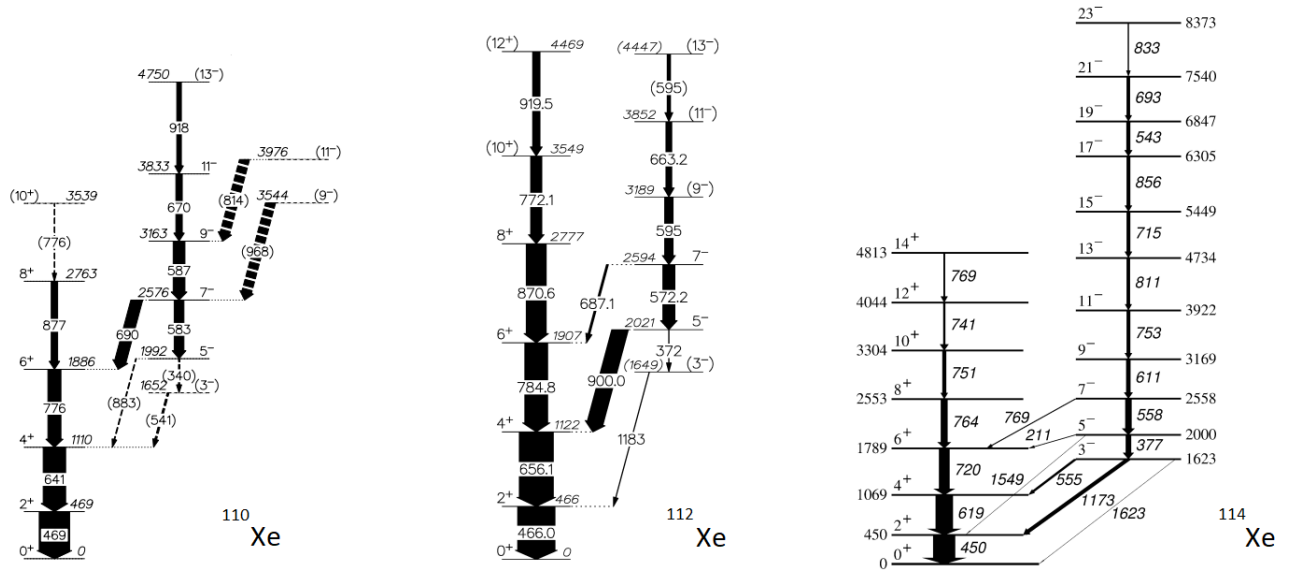

Figure 19: Comparison between the level schemes of the N=56 ^{110}Xe, N=58 ^{112}Xe [23] and N=60 ^{114}Xe [3] isotopes. The energies of the levels are not in scale between the three isotopes.

In Fig. 20 the ground state and octupole band are presented in energy scale. Surprisingly ^{110}Xe energy levels differ at most by $\simeq$ 50 keV from ^{112}Xe ones, while for ^{114}Xe, except for the 8^+ and 10^+ states, they are compatible within 100 keV.

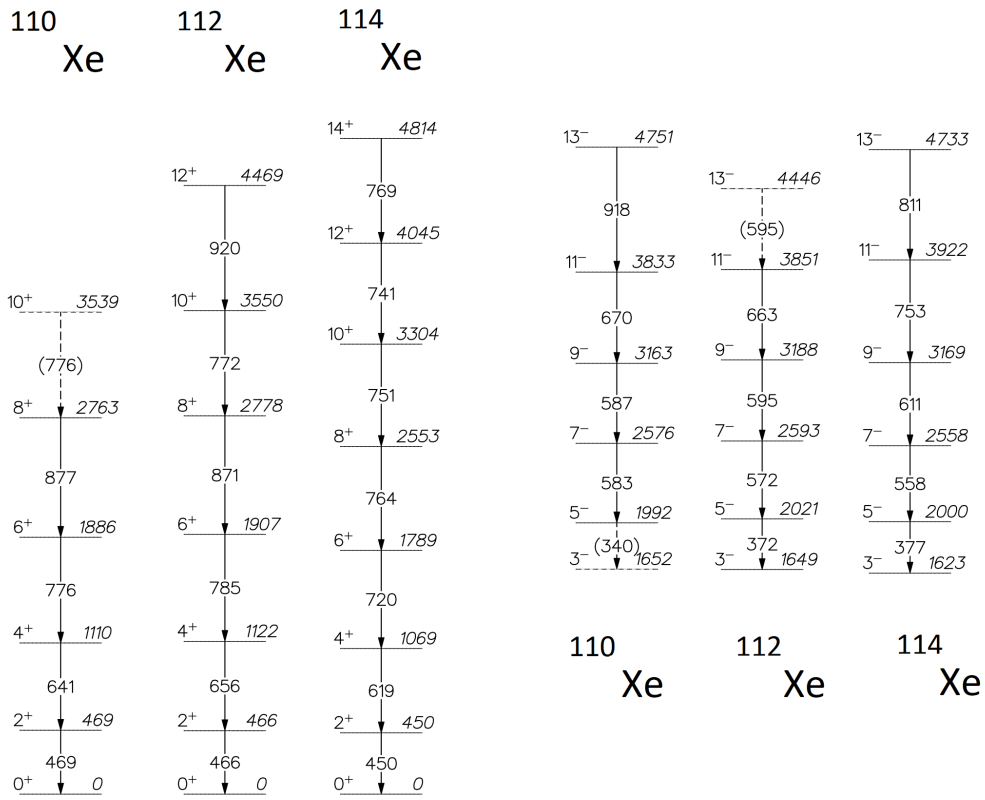

Figure 20: Comparison between the energies and J^{π} for the ground state and octupole band of ^{110}Xe, ^{112}Xe and ^{114}Xe. The intensity is set to zero for all the transitions.

In addition to the γ transitions belonging to the ground state and octupole band, two other very intense γ rays have been identified, with energy 813.6(3) keV and 968.3(3) keV, in the ^{110}Xe level scheme. Fig. 21 shows the complete level scheme of ^{114}Xe [28], where two intense transitions with energy 693 keV and 730 keV can be seen. These might correspond to the 813.6(3) keV and 968.3(3) keV γ rays observed for ^{110}Xe, in agreement with the $\gamma\gamma$ coincidences analysis.

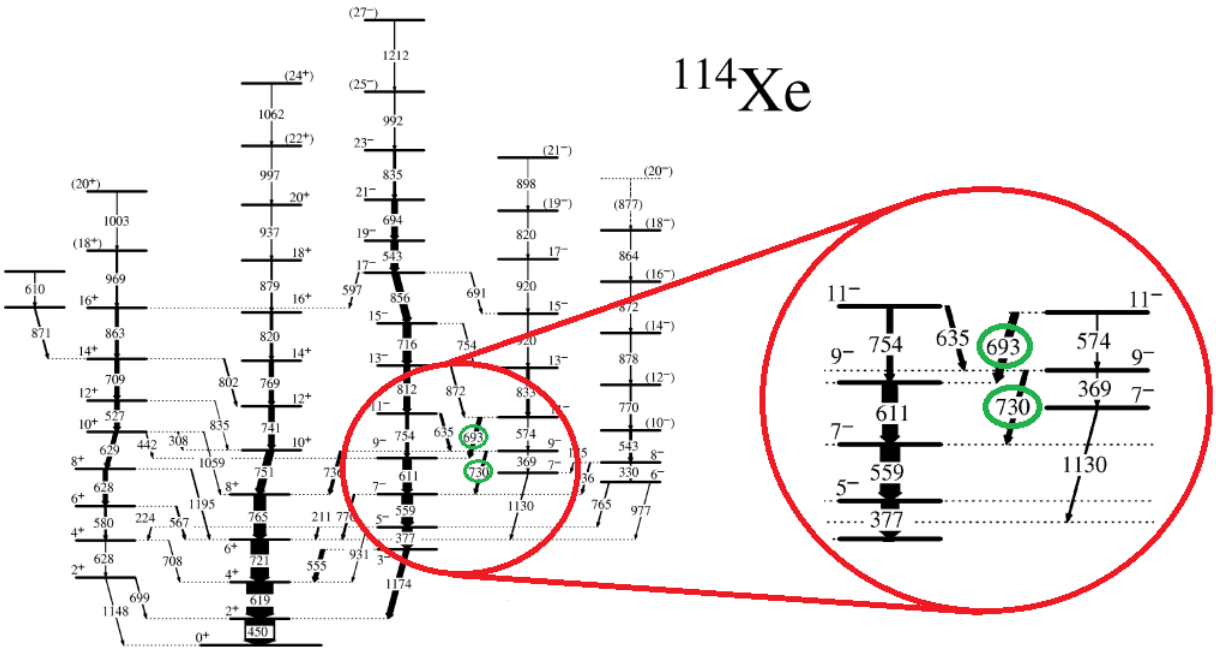

Figure 21: Complete level scheme of ^{114}Xe, from [28], used for the J^{π} assignment of 813.6(3) keV and 968.3(3) keV γ rays in the ^{110}Xe level scheme. The corresponding γ transitions are circled in green.

Furthermore, in the ^{112}Xe nucleus two transitions not placed in the level scheme and with similar energies have been observed [23]. Fig. 22 shows two peaks with energies 964 keV (top spectrum) and 818 keV (bottom spectrum) that might correspond to the γ decays respectively from the 9^- and 11^- states, respectively. Indeed these transitions are observed when gating respectively on the $7^- \rightarrow 5^-$ 572 keV and $9^- \rightarrow 7^-$ 595 keV γ rays. These transitions might be the counterpart of the 813.6(3) keV and 968.3(3) keV γ rays, with very similar energies, observed for ^{110}Xe .

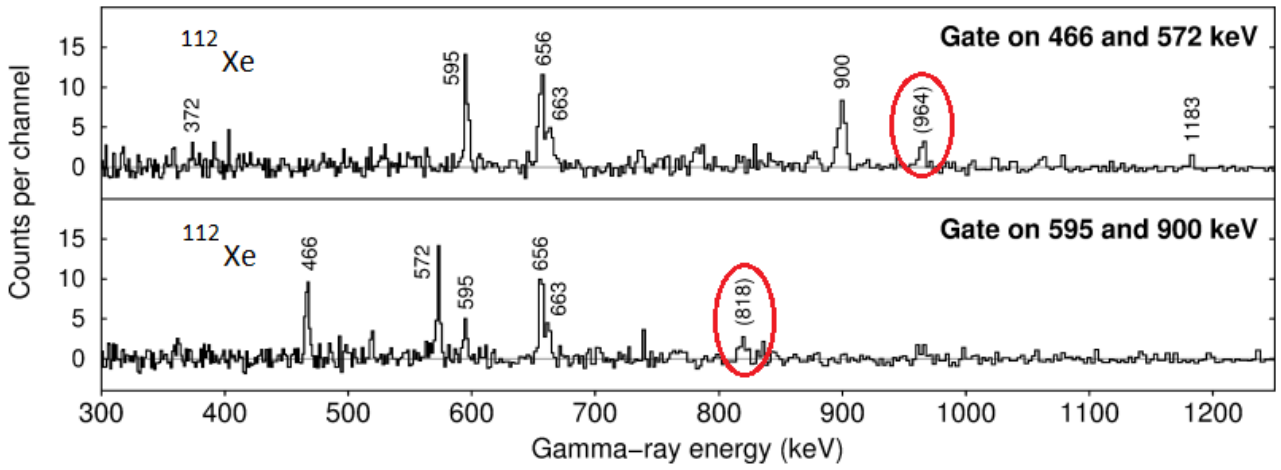

Figure 22: Gated spectra for ^{112}Xe, adapted from [23], with the two transitions circled in red corresponding to the 813.6(3) keV and 968.3(3) keV in the ^{110}Xe level scheme.

5 Summary and Perspectives

In this thesis the proton rich ^{110}Xe was studied. This nucleus was produced via the ^{54}Fe(^{58}Ni,2n) fusion-evaporation reaction at the Accelerator laboratory of the University of Jyväskylä (Finland) in 2020. The reaction products were separated in-flight from the beam particles using the MARA recoil mass separator and the ^{110}Xe was then implanted into a DSSD. The in-beam γ rays emitted from the excited ^{110}Xe levels were measured by the Jurogam Phase-III γ spectrometer. Given the low cross-section of the reaction under study, the $\alpha\alpha$ recoil decay tagging technique was used in order to obtain a clean in-beam γ-ray spectrum. We extended the level scheme of ^{110}Xe analysing the $\gamma\gamma$ coincidence relationships and the relative intensities between the transitions. The ground state band was built up to the 10^+ state, while the octupole band was identified for the first time up to the 13^- state. Finally, the comparison with the neighbouring even-even Xe isotopes showed similar behaviours in their level scheme structure, allowing spin and parity assignments to the energy levels of ^{110}Xe.

The limited statistics available did not allow the identification of additional levels and transitions, as for example the $3^- \rightarrow 0^+$ transition, which would represent a clear benchmark of the octupole deformation in ^{110}Xe. Indeed, assuming for the latter a relative intensity similar to the ^{114}Xe case ($\simeq$0.1%), in order to definitely establish its presence in ^{110}Xe level scheme the statistics should be increased by a factor of 5. In addition, this improvement would allow a more precise angular distribution analysis and, as a result, conclusive results regarding the multipolarity of the most intense transitions would be drawn. The proposed improvement can be achieved, for example, by improving the efficiency of both the γ-ray array and the focal plane detectors. Moreover, increasing the beam intensity would be possible to improve the quality of the spectra and draw definitive conclusions regarding ^{110}Xe level scheme.

Currently, detailed theoretical calculations are ongoing in order to have a complete description of the octupole correlations in ^{110}Xe and eventually in the full isotopic chain of the neutron-deficient Xe isotopes [29].

References

[1] P. A. Butler and W. Nazarewicz. Intrinsic reflection asymmetry in atomic nuclei. *Rev. Mod. Phys.*, 68:349–421, Apr 1996.

[2] Bing-Nan Lu, En-Guang Zhao, and Shan-Gui Zhou. Potential energy surfaces of actinide nuclei from a multidimensional constrained covariant density functional theory: Barrier heights and saddle point shapes. *Phys. Rev. C*, 85:011301, Jan 2012.

[3] G. de Angelis et al. Coherent proton–neutron contribution to octupole correlations in the neutron-deficient ^{114}Xe nucleus. *Phys. Lett. B*, 535:93–102, 2002.

[4] K. Nomura, L. Lotina, T. Nikšić, and D. Vretenar. Microscopic description of octupole collective excitations near N=56 and N=88. *Phys. Rev. C*, 103(5), May 2021.

[5] M. Sandzelius et al. Identification of Excited States in the $T_z = 1$ Nucleus ^{110}Xe: Evidence for Enhanced Collectivity near the $N = Z = 50$ Double Shell Closure. *Phys. Rev. Lett.*, 99:022501, Jul 2007.

[6] A. Korgul, K. P. Rykaczewski, C. J. Gross, R. K. Grzywacz, S. N. Liddick, C. Mazzocchi, J. C. Batchelder, C. R. Bingham, I. G. Darby, C. Goodin, J. H. Hamilton, J. K. Hwang, S. V. Ilyushkin, W. Królas, and J. A. Winger. Toward ^{100}Sn: Studies of excitation functions for the reaction between ^{58}Ni and ^{54}Fe ions. *Phys. Rev. C*, 77:034301, Mar 2008.

[7] J. Sarén et al. The new vacuum-mode recoil separator MARA at JYFL. *Nucl. Instr. Meth. B*, 266:4196–4200, 2008.

[8] Rémi N. Bernard, Luis M. Robledo, and Tomás R. Rodríguez. Octupole correlations in the ^{144}Ba nucleus described with symmetry-conserving configuration-mixing calculations. *Phys. Rev. C*, 93:061302, Jun 2016.

[9] T.R. Rodríguez. *Private communication.*

[10] K. Auranen. Spectroscopy of ^{199,201}At. PhD Thesis, University of Jyväskylä, 2015.

[11] J. Pakarinen, J. Ojala, P. Ruotsalainen, et al. The jurogam 3 spectrometer. *Eur. Phys. J. A*, 56, 05 2020.

[12] C. W. Beausang, S. A. Forbes, P. Fallon, P. J. Nolan, P. J. Twin, J. N. Mo, J. C. Lisle, M. A. Bentley, J. Simpson, F. A. Beck, D. Curien, G. deFrance, G. Duchêne, and D. Popescu. Measurements on prototype Ge and BGO detectors for the Eurogam array. *Nucl. Instr. Meth. A*, 313(1):37–49, March 1992.

[13] G. Duchêne, F. A. Beck, P. J. Twin, G. de France, D. Curien, L. Han, C. W. Beausang, M. A. Bentley, P. J. Nolan, and J. Simpson. The Clover: a new generation of composite Ge detectors. *Nucl. Instr. Meth. A*, 432(1):90–110, August 1999.

[14] http://www.micronsemiconductor.co.uk.

[15] H. Joukainen et al. *In preparation.*

[16] I.H. Lazarus et al. The GREAT triggerless total data readout method. *IEEE Trans. Nucl. Sci.*, 48:567, 2001.

[17] https://radware.phy.ornl.gov/gf3/5.3.

[18] E. S. Paul, P. J. Woods, T. Davinson, R. D. Page, P. J. Sellin, C. W. Beausang, R. M. Clark, R. A. Cunningham, S. A. Forbes, D. B. Fossan, A. Gizon, J. Gizon, K. Hauschild, I. M. Hibbert, A. N. James, D. R. LaFosse, I. Lazarus, H. Schnare, J. Simpson, R. Wadsworth, and M. P. Waring. In-beam gamma-ray spectroscopy above ^{100}Sn using the new technique of recoil decay tagging. *Phys. Rev. C*, 51:78–87, 1995.

[19] Z. Janas, C. Mazzocchi, L.Z. Batist, et al. Measurements of ^{110}Xe and ^{106}Te decay half-life. *Eur. Phys. J. A*, 23:197–200, 2005.

[20] A. Gavron. Statistical model calculations in heavy ion reactions. *Phys. Rev. C*, 21:230–236, 1980.

[21] O.B. Tarasov and D. Bazin. LISE++: Radioactive beam production with in-flight separators. *Nucl. Instr. Meth. B*, 266:4657–4664, 2008.

[22] http://bricc.anu.edu.au/index.php.

[23] J. F Smith et al. Excited states and deformation of ^{112}Xe. *Phys. Lett. B*, 523:13–21, 2001.

[24] H. Morinaga and T. Yamazaki. *In-Beam Gamma-Ray Spectroscopy.* Elsevier Science Ltd, 1976.

[25] K. Siegbahn. *Alpha-, beta- and gamma-ray spectroscopy.* North-Holland, 1965.

[26] C. Wheldon. K-isomerism at high-spin beyond the fusion limit. PhD Thesis, University of Surrey, 1999.

[27] M. G. Procter, T. Bäck, B. Cederwall, et al. Electromagnetic transition strengths in $^{109}_{52}$Te. *Phys. Rev. C*, 86:034308, 2012.

[28] E. S. Paul et al. High-spin study of neutron-deficient ^{114}Xe. *Nucl. Phys. A*, 673:31–44, 2000.

[29] T.R. Rodríguez, A. Poves, L. Robledo. *Private communication.*